Journal of Power Sources 244 (2013) 515–520

Contents lists available at SciVerse ScienceDirect

Journal of Power Sources

journal homepage: www.elsevier.com/locate/jpowsour

Short communication

Influence of the crystallographic orientation of silicon nanowires in a carbon matrix on electrochemical performance as negative electrode materials for lithium-ion batteries

Seong-Ho Baek, Jung-Soo Park, Eun-Jin Bae, Yong-Il Jeong, Bum-Young Noh, Jae Hyun Kim*

Division of Green Energy Research, Daegu-Gyeongbuk Institute of Science and Technology (DGIST), 50-1, Sang-Ri, Hyeonpung-Myeon, Dalseong-gun, Daegu 711-873, Republic of Korea

HIGHLIGHTS

- The electrochemical performance of SiNW depending on substrate orientation was investigated.
- The discharge capacity of <110>-SiNWs was greatly improved with an increasing carbon/SiNWs ratio.
- Large amount of carbon accommodates the volume expansion of SiNW and increased the electronic conductivity.

ARTICLE INFO

Article history:
Received 11 October 2012
Received in revised form
12 February 2013
Accepted 15 February 2013
Available online 26 February 2013

Keywords:
Lithium ion batteries
Silicon nanowire
Negative electrode materials
Metal-assisted chemical etching
Carbon matrix

ABSTRACT

In this study, we report the effect of the crystallographic orientation of silicon nanowires (SiNWs) on electrochemical performance as a negative electrode material. We synthesize vertically aligned SiNWs from differently oriented Si substrates with axial orientations of Si <100>, <110>, and <111> by the metal-assisted chemical etching method. To investigate the influence of a carbon matrix on SiNWs, various ratios of carbon/SiNWs are incorporated into negative electrode materials. The electrochemical performance of the <110>-SiNWs is greatly improved by increasing the carbon/SiNWs ratio from 0.5 to 2 compared to <100> and <111>-SiNWs. The electrochemical results reveal that a reversible capacity of more than 3200 mAh g^{-1} at a current rate of 0.1 C was obtained by using <110>-SiNWs with a carbon/SiNWs ratio of 2. The enhanced electrochemical performance is attributed to the relatively large interspacing between atoms along the <110> direction, which is much larger than those along the <100> and <111> directions. We also suggest that a large amount of carbon accommodates the volume expansion that occurs during the Li alloying/dealloying processes with Si and increases the electronic conductivity.

1. Introduction

Recently, the lithium ion battery (LIB) has been regarded as one of the most promising energy storage devices for portable electronics and electric-powered automotive applications [1,2]. To satisfy the increasing power demands for many applications, significant research challenges and opportunities exist for all types of battery materials, such as conversion oxides [1], silicon (Si) [3–7], and carbon [8]. Among them, Si has been considered a promising negative electrode material for LIBs to replace carbonaceous materials. Si is a readily available, non-hazardous material that can be refined into an extremely pure form with a large mass. Furthermore, a large amount of Li has been incorporated into Si, which resulted in a negative electrode capacity of 4200 mAh g^{-1}, which is 10 times larger than the capacity of graphite negative electrodes [9–13]. A bulk Si negative electrode exhibits a high specific capacity in the initial stages, but the cycle performance is likely to decay rapidly due to pulverization with increasing cycle numbers [14]. More recently, nanostructured Si negative electrodes have been shown to exhibit excellent performance to take advantage of Si's superior fracture resistance and direct pathway for efficient charge transport [15–22].

A few studies have reported that preferential volume changes were found in SiNWs during Li alloying–dealloying processes with Si [23–26]. Lee et al. claimed that the crystalline Si structure along the <110> direction produces large interstitial spaces between atoms, which gives rise to a high-speed Li ion diffusion channel [23]. Liu et al. observed anisotropic swelling of SiNWs during lithiation and revealed that such anisotropic expansion is due to the

* Corresponding author. Tel.: +82 53 785 3610; fax: +82 53 785 3439.
E-mail address: jaehyun@dgist.ac.kr (J.H. Kim).

0378-7753/$ – see front matter © 2013 Elsevier B.V. All rights reserved.
http://dx.doi.org/10.1016/j.jpowsour.2013.02.053

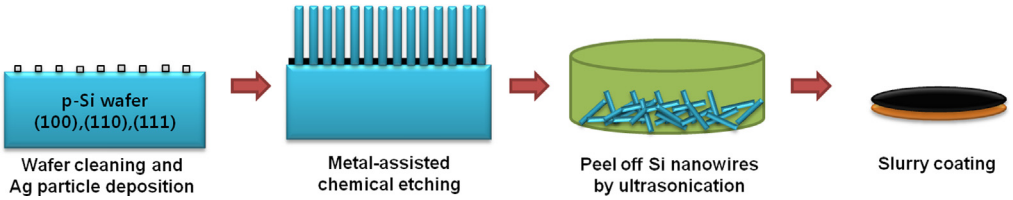

Fig. 1. Schematic illustration of the fabrication of SiNW negative electrodes.

interfacial processes of relaxing strains at the reaction front depending on crystallographic orientation [24]. Zhang et al. studied anisotropic Li intercalation behavior with different types of SiNWs, including binding energy, diffusion barriers, and strain effects [25]. In addition, a chemomechanical model was introduced to study the phase evolution and morphological changes in lithiated SiNWs [26].

However, to the best of our knowledge, the relationship between the orientation of SiNWs and their electrochemical properties has not been reported in the literature so far. In this study, we made a SiNWs-based electrode to investigate the effect of the crystallographic orientation of SiNWs on their electrochemical performance using the traditional slurry method. In addition, our efforts focused on relaxing large volume changes by mixing SiNWs with inactive carbon to prevent fracturing of the SiNWs and to act as a conductive medium for the charge carrier between the SiNW negative electrode and the current collector.

2. Experimental

2.1. Synthesis of SiNWs

SiNW arrays were synthesized via the metal-assisted chemical etching of boron-doped Si wafers with a resistivity in the range of 1–10 Ωcm. Four-inch Si wafers with three different orientations, namely, (100), (110), and (111), were used in this study. The whole Si wafers were immersed in a boiling solution of NH_4OH (30%)/H_2O_2 (30%)/H_2O (1:1:5) at 60 °C for 30 min, which removed organic contaminants and native oxide. Then, the wafers were rinsed thoroughly with deionized (DI) water. The Si etching procedure comprised two steps [27,28]. First, silver nanoparticles (AgNPs) were deposited on the Si wafer pieces by electroless plating, during which the wafers were immersed in an aqueous mixture of 0.02 M silver nitrate ($AgNO_3$) and 4.6 M hydrofluoric acid (HF) for 1 min. In the second step, the wafer pieces covered with AgNPs were immersed in an etchant solution containing 4.6 M HF and 0.44 M H_2O_2 in the volume ratio of 1:1. The wafers were kept in the solution in a Teflon bath for 15 min at room temperature. AgNPs were removed by nitric acid and cleaned by rinsing with DI water, and air drying. The SiNW arrays were separated from the mother Si wafer by ultrasonication for 10 min in ethanol.

2.2. Preparation of electrodes and cell assembly

The electrodes were prepared by coating slurries containing the SiNW active materials, acetylene black (Super P) and

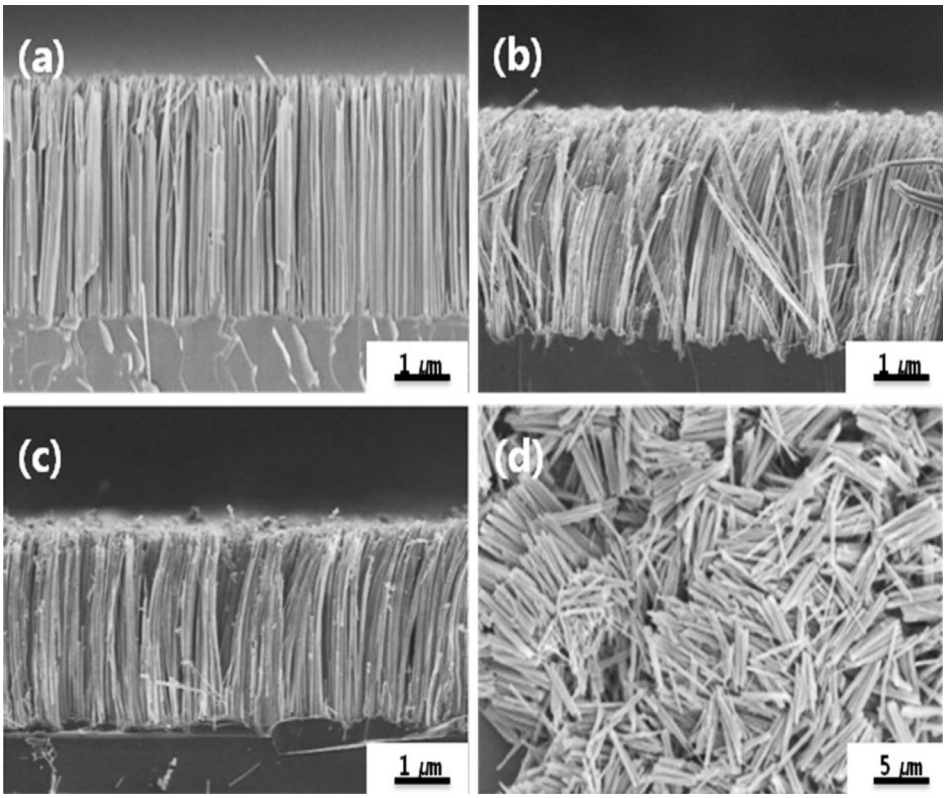

Fig. 2. SEM images of SiNWs with three different axial orientations: (a) <100>, (b) <110>, (c) <111> and (d) separated SiNWs.

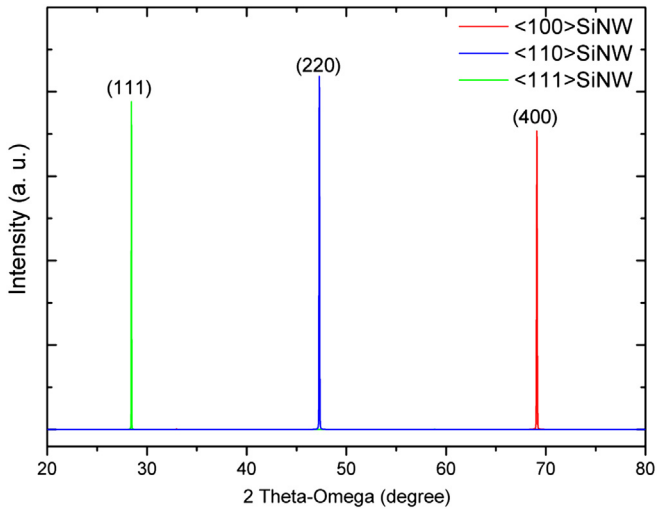

Fig. 3. 2Theta–omega scan of SiNWs on bulk Si substrate with three different axial orientations.

polyvinylidene fluoride (PVDF), by milling with an agate mortar at volumetric ratios of 3:6:1, 4.5:4.5:1, and 6:3:1. The slurry was then spread onto a current collector of copper foil using a doctor blade technique and dried in a vacuum oven at 110 °C for 12 h. CR2032-type coin cells were used to test the electrochemical performance of the samples. The electrolyte consisted of 1 M of $LiPF_6$ in a non-aqueous solution of ethylene carbonate (EC)/dimethyl carbonate (DMC) with a volume ratio of 1:1 (Panaxetec. Inc). A Celgard 2400 microporous membrane was used as a separator in the coin cell. Li metal was used as a counter electrode. The cells were assembled in an Ar-filled glove box with concentrations of moisture and oxygen below 1 ppm.

2.3. Characterization

The morphological properties of all the samples were characterized by scanning electron microscopy (SEM, Hitachi-S4800). X-ray diffraction (XRD, Panalytical Empyrean) was used to observe the crystallographic structures. A galvanostatic cycling test was carried out at various constant current densities between 0.01 and 1.5 V vs. Li/Li^+ with a TOSCAT 3100 battery tester (Toyo system). All the specific capacities of the samples were calculated on the basis of the weight of the active materials. The electrochemical impedance spectra were measured from 100 kHz to 0.01 Hz with an alternating current amplitude of 10 mV using a VersaSTAT3 potentiostat (Princeton Applied Research).

3. Results and discussion

Fig. 1 shows the fabrication processes for making a negative electrode with SiNW arrays, which is described in detail in the Experimental section. Fig. 2(a)–(c) shows cross-sectional SEM images of the SiNW arrays fabricated by the metal-assisted chemical etching method. It should be noted that all the SiNWs were perpendicular to the surface of the Si wafer, which is along the direction normal to the original substrate with various orientations. These results show that AgNPs tend to move vertical to the Si substrate (Fig. 2(a)–(c)) during metal-assisted chemical etching. We concluded that the site-selective redox reaction occurred only between AgNPs and the exposed parts of the Si wafer. Thus, when AgNP-loaded substrates with different $AgNO_3$ concentrations were etched in the mixed solution of 4.6 M HF and 0.04 M H_2O_2, the arrayed SiNWs formed on the Si surface with the reduction of

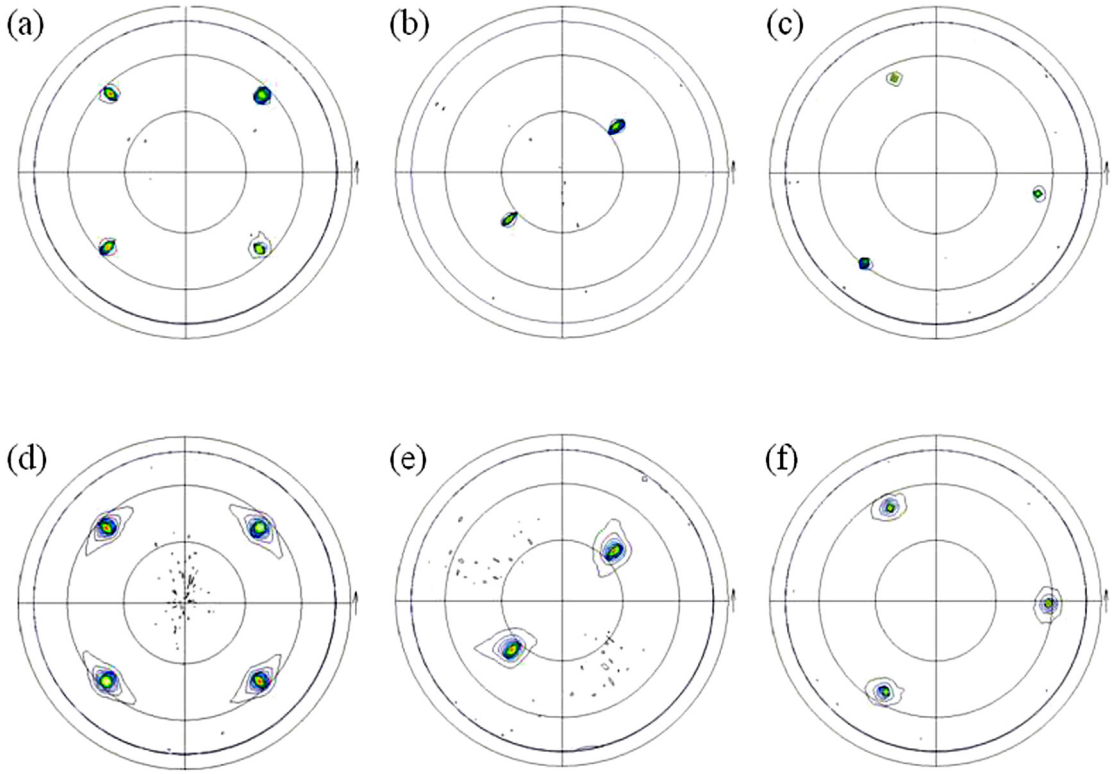

Fig. 4. Pole figures of bulk Si substrates of (a) <100>, (b) <110>, and (c) <111>. Pole figures of SiNW arrays on bulk substrates are sequentially corresponding to (d–f), respectively.

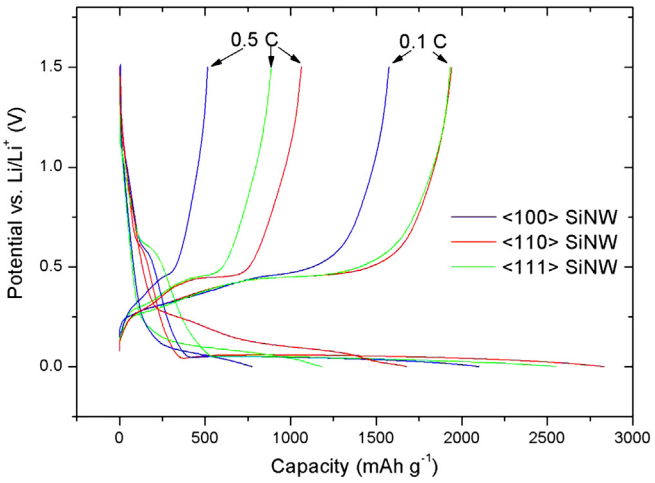

Fig. 5. The first charge–discharge curves of SiNWs as the negative electrode with a carbon/Si ratio of 1 at different c-rates.

AgNPs by the oxidation of Si, thereby forming SiO_2 which was dissolved in the HF surroundings [27,28]. SEM images showed that the arrays of pristine SiNWs had approximately a 10 μm length and diameters of 50–100 nm. The aligned SiNWs were dispersed in ethanol by ultrasonication and peeled off from the mother substrate as shown in Fig. 2(d).

To examine the structural properties of the SiNWs, XRD measurements were carried out on the SiNW arrays on bulk Si substrates. First, 2θ–ω scan measurements were performed on these samples to detect the SiNW phase from the equally oriented bulk Si. As shown in Fig. 3, only (*hkl*) peaks related to the Bragg diffraction condition of bulk substrate were observed for all samples, and no other peak or broadening was detected. To distinguish the orientation of SiNWs and bulk Si, X-ray pole figure measurements were conducted. The X-ray pole figure for a particular (*hkl*) plane describes the statistical angular distribution of the direction of the normal to the chosen (*hkl*) plane [29]. We can place the samples in the center of an imaginary hemisphere for each crystallite, making the intersection between the normal to the chosen (*hkl*) plane and the sphere [30]. By projecting the density of marks on the sphere onto the planar surface, we obtained the (*hkl*) pole figure for each sample. From the {111} pole figure for the Si (100) bulk substrate, four points were observed in the {111} pole figure as shown in Fig. 4(a). However, for the {111} pole figure of the SiNWs on the Si (100) substrate, the four poles were broadened according to the tilt angles, while its four pole symmetry was maintained (Fig. 4(d)). This means that the SiNW arrays have the same orientation as the bulk substrate, but they have a slightly tilted distribution of crystallites to the pole figure direction. These results were similar to the {111} pole figure of Si (110) and the {004} pole figure of (111) substrate and the SiNWs in Fig. 4(b,e) and (c,f), respectively. Therefore, we suggest that the SiNW arrays mostly stand vertical to the bulk substrates and retain their orientation from the mother substrates.

Then, to investigate the electrochemical performance of differently oriented SiNW arrays, CR2032 coin cells using SiNWs as negative electrodes by the slurry coating method were assembled with Li metal foil as the counter electrode. Fig. 5 shows the voltage profiles of the SiNW negative electrode in the charge (delithiation) and discharge (lithiation) process in a potential window of 0.01–1.5 V vs Li^+/Li. As shown in Fig. 5, the first discharge capacity of the <110> SiNW negative electrode increased with an increase of current rate more than that of the <100> and <111> SiNWs. It is considered that Li ions rapidly diffuse along the <110> direction, which causes preferential volume expansion along this direction [23–26].

Carbon materials have been generally used as the buffer matrix because they exhibit less structural change than Si and mechanical supports [31–36]. Carbon networks also enable efficient transfer of electrons to the SiNWs. Thus, we tested nanostructured Si–carbon composites by varying the carbon/Si ratio. Fig. 6 shows the

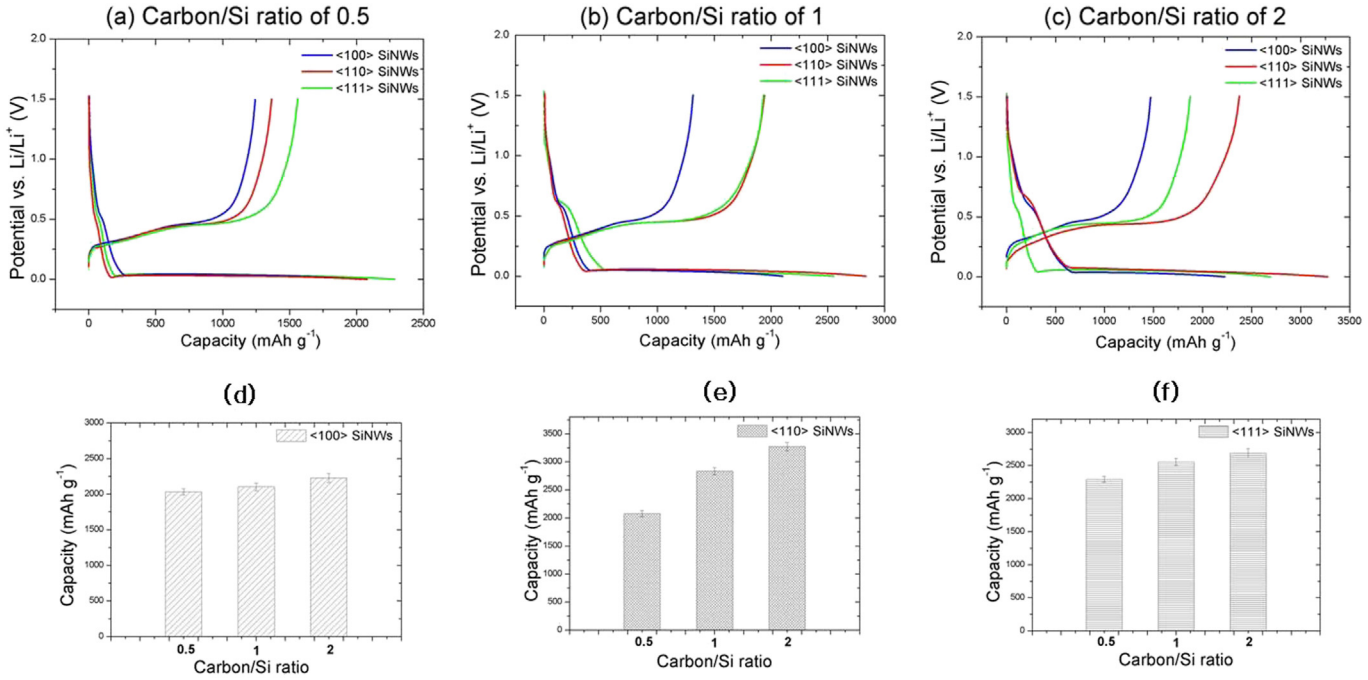

Fig. 6. The first charge–discharge curves of SiNWs as the negative electrode at a carbon/Si ratio of (a) 0.5, (b) 1, and (c) 2. Capacity changes of SiNWs with an axial orientation of (d) <100>, (e) <110>, and (f) <111>.

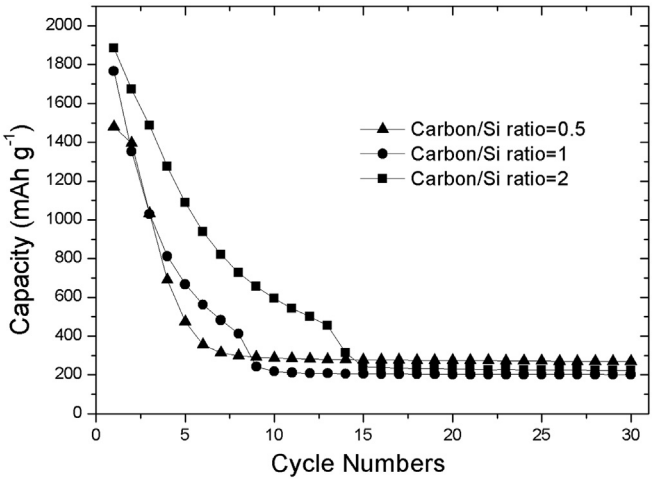

Fig. 7. Comparison of cyclability of <110>-SiNWs at carbon/Si ratios from 0.5 to 2.

relationships between the specific capacity of the SiNW negative electrode and the carbon content during charge–discharge. As shown in Fig. 6(a)–(c), the capacity change of the <110> SiNWs greatly increased with an increase in the carbon/Si ratio. This means that a large amount of carbon mechanically accommodated the volume expansion of the <110> SiNW negative electrode, which did not occur in the <100> and <111> SiNWs. As shown in Fig. 6(d)–(f), the changes in the discharge capacity with a varying carbon/Si ratio from 0.5 to 2 were 9.5% for <100>-SiNWs, 57% for <110>-SiNWs, and 17% for <111>-SiNWs. This provides evidence that carbon materials act as a buffer matrix to prevent the agglomeration of SiNW bundles and restrain volume expansion. In other words, when the content of carbon is lower than that of SiNWs, the specific capacity begins to decrease due to the deterioration of active materials, as shown in Fig. 6(a).

Fig. 7 shows the discharge capacity of each sample as a function of cycle numbers at the rate of 0.5 C, which indicates the cycle ability of the nanostructured Si–C composite electrodes. Clearly, the capacity retention of the <110>-SiNW negative electrode with a carbon/Si ratio of 2 is higher than that of the other samples in the initial stages. The better cycling ability is attributed to the improved conductivity and relaxed mechanical stresses. However, the specific capacities of all samples rapidly faded in the following cycles regardless of the carbon/Si ratio. This poor cycle ability can be ascribed to large volumetric expansion as Si converts to $Li_{15}Si_4$ in a highly anisotropic transformation [24]. Moreover, a binder that has a significant impact on the electrochemical performance of Si-based electrodes was reported. Recent results have shown that a relatively low Si content and sodium carboxymethyl cellulose (CMC) binders perform better than PVDF binders in Si-based electrodes for hundreds of cycles [37,38]. Thus, how to achieve a highly improved cycle performance is still under investigation.

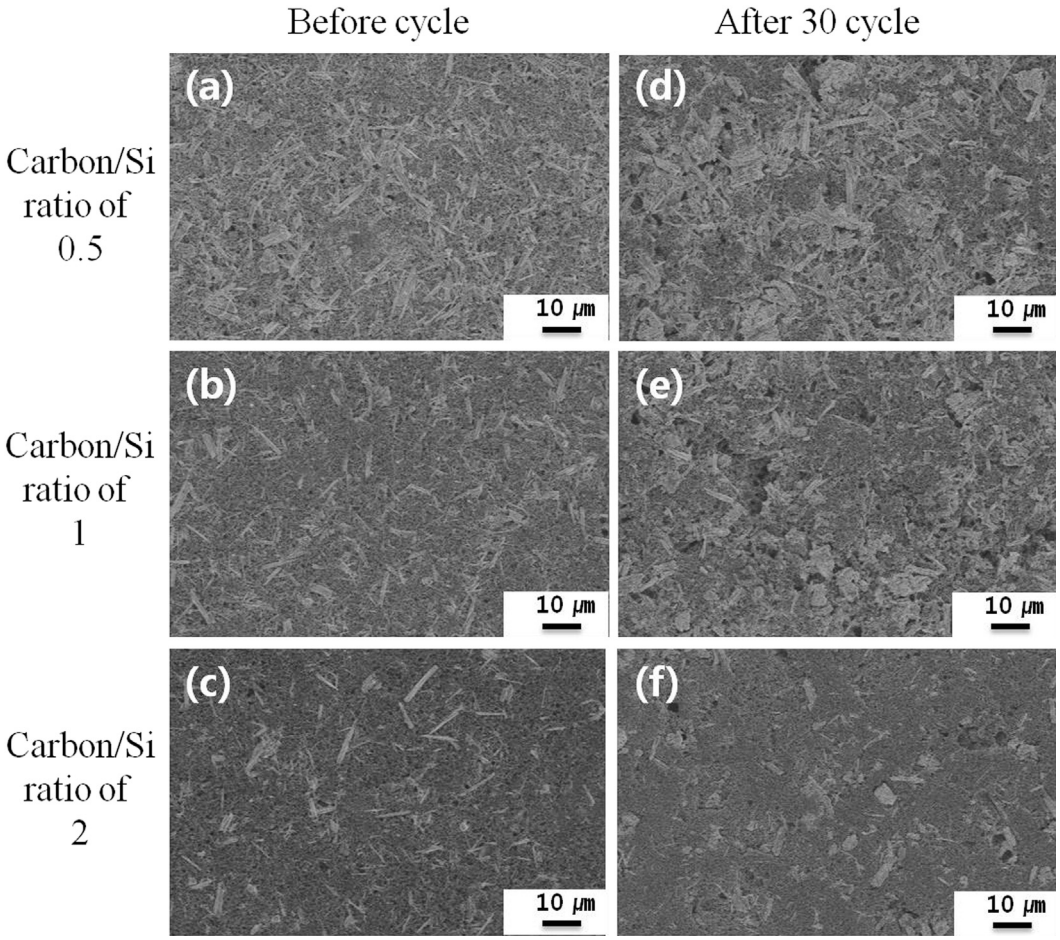

Fig. 8. SEM images of <110> SiNW electrodes before the cycle test at a carbon/Si ratio of (a) 0.5, (b) 1, and (c) 2. SEM images of <110> SiNW electrodes after 30 cycles are sequentially correspond to (d)–(f), respectively.

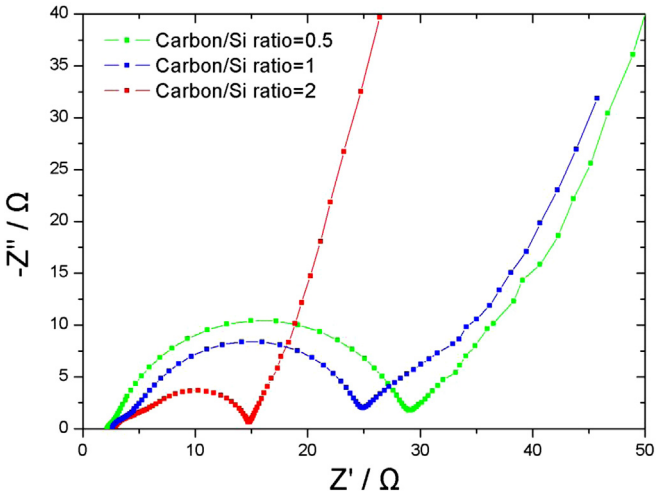

Fig. 9. Electrochemical impedance spectra of <110> SiNW electrodes at carbon/Si ratios from 0.5 to 2.

Fig. 8 shows the SEM image of <110> SiNW–carbon composites with varying carbon/Si ratios before and after 30 charge–discharge cycles. It should be noted that the morphology after 30 cycles (Fig. 8(a)–(c)) was completely different from that of the original negative electrodes (Fig. 8(d)–(f)). We observed that the volume expansion of SiNWs is mainly related to diameter swelling along the <110> axial direction. With a decreasing carbon/Si ratio, the carbon matrix around the SiNWs peeled off from its position and created a void, indicating that the Si expansion totally destroyed the carbon structure after the cycling test. However, with increased buffer materials, the expected capacity increased. Therefore, the first discharge capacities of the Si/C composites increased. The presence of a buffer material is desirable to suppress the structure destruction of the carbon framework, and it enables better accommodation of volume expansion.

Fig. 9 shows the AC impedance spectra of the electrodes of the <110>-SiNW negative electrode with an increasing carbon/Si ratio. Semicircular arcs can be assigned to the charge transfer impedance of the electrodes. The depressed semicircles in the high-frequency and medium frequency regions are assigned to the solid electrolyte interface (SEI) film and the interfacial charge-transfer impedance, respectively, while the inclined line in the low frequency region is attributed to the Li ion diffusion impedance. The semicircle shows that interfacial impedance decreased with an increase of carbon content, suggesting that the electrical conductivity with a high carbon/Si ratio is much larger than that with a low carbon/Si ratio.

4. Conclusions

In summary, we investigated the influences of the crystallographic orientation of SiNWs on electrochemical performance using the slurry coating method. The first discharge capacity of the <110> SiNW negative electrode was higher than that of the <100> and <111> SiNWs. We attributed this to the Li ions rapidly diffusing along the <110> direction, which causes preferential volume expansion along this direction. We also found that the carbon content in crystalline SiNW negative electrode plays an important role. A carbon matrix helps to suppress the volume expansion and aggregation of SiNW active materials during the lithiation–delithiation process. Moreover, carbon networks act as conducting media with efficient electron transfer. Developing SiNW negative electrodes by combination of a {110} facet and a buffer matrix is a new strategy for the design of high-power and high energy-density devices.

Acknowledgment

This work was financially supported by a basic research program (11-EN-03) through the Daegu-Gyeongbuk Institute of Science and Technology (DGIST) funded by the Ministry of Education, Science and Technology (MEST). Authors acknowledge Dr. Sang Geul Lee at the Korea Basic Science Institution (KBSI) in Daegu for useful discussion and taking the XRD data.

References

[1] J.M. Tarascon, M. Armand, Nature 414 (2001) 359–367.
[2] R.F. Service, Science 332 (2011) 1494–1496.
[3] J.O. Besenhard, J. Yang, M. Winter, J. Power Sources 68 (1997) 87–90.
[4] T.D. Hatchard, J.R. Dahn, J. Electrochem. Soc. 151 (2004) A838–A842.
[5] W.J. Weydanz, M. Wohlfahrt-Mehrens, R.A. Huggins, J. Power Sources 81 (1999) 237–242.
[6] X.W. Zhang, P.K. Patil, C. Wang, A.J. Appleby, F.E. Little, D.L. Cocke, J. Power Sources 125 (2004) 206–213.
[7] W.J. Zhang, J. Power Sources 196 (2011) 13–24.
[8] B. Scrosati, J. Garche, J. Power Sources 195 (2010) 2419–2430.
[9] U. Kasavajjula, C.S. Wang, A.J. Appleby, J. Power Sources 163 (2007) 1003–1039.
[10] B.A. Boukamp, G.C. Lesh, R.A. Huggins, J. Electrochem. Soc. 128 (1981) 725–729.
[11] B. Key, R. Bhattacharyya, M. Morcrette, V. Seznec, J.M. Tarascon, C.P. Grey, J. Am. Chem. Soc. 131 (2009) 9239–9249.
[12] R.A. Huggins, J. Power Sources 81 (1999) 13–19.
[13] C.M. Park, J.H. Kim, H. Kim, H. Sohn, J. Chem. Soc. Rev. 39 (2010) 3115–3141.
[14] J. Qu, H. Li, J. Henry, S.K. Martha, N.J. Dudney, H. Xu, M. Chi, M.J. Lance, S.M. Mahurin, T.M. Besmann, S. Dai, J. Power Sources 198 (2012) 312–317.
[15] C.K. Chan, H.L. Peng, G. Liu, K. McIlwrath, X.F. Zhang, R.A. Huggins, Y. Cui, Nat. Nanotechnol. 3 (2008) 31–35.
[16] L.F. Cui, R. Ruffo, C.K. Chan, H.L. Peng, Y. Cui, Nano Lett. 9 (2009) 491–495.
[17] B. Hertzberg, A. Alexeev, G. Yushin, J. Am. Chem. Soc. 132 (2010) 8548–8549.
[18] H. Kim, B. Han, J. Choo, J. Cho, Angew. Chem. Int. Ed. 47 (2008) 10151–10154.
[19] A. Esmanski, G.A. Ozin, Adv. Funct. Mater. 19 (2009) 1999–2010.
[20] A. Magasinski, P. Dixon, B. Hertzberg, A. Kvit, J. Ayala, G. Yushin, Nat. Mater. 9 (2010) 353–358.
[21] M.H. Park, M.G. Kim, J. Joo, K. Kim, J. Kim, S. Ahn, Y. Cui, J. Cho, Nano Lett. 9 (2009) 3844–3847.
[22] Y.Q. Zhang, X.H. Xia, X.L. Wang, Y.J. Mai, S.J. Shi, Y.Y. Tang, C.G. Gu, J.P. Tu, J. Power Sources 213 (2012) 106–111.
[23] S.W. Lee, M.T. McDowell, J.W. Choi, Y. Cui, Nano Lett. 11 (2011) 3034–3039.
[24] X.H. Liu, H. Zheng, L. Zhong, S. Huang, K. Karki, L.Q. Zhang, Y. Liu, A. Kushima, W.T. Liang, J.W. Wang, J.-H. Cho, E. Epstein, S.A. Dayeh, S.T. Picraux, T. Zhu, J. Li, J.P. Sullivan, J. Cumings, C. Wang, S.X. Mao, Z.Z. Ye, S. Zhang, J.Y. Huang, Nano Lett. 11 (2011) 3312–3318.
[25] Q. Zhang, Y. Cui, E. Wang, J. Phys. Chem. 115 (2011) 9376–9381.
[26] H. Yang, S. Huang, X. Huang, F. Fan, W. Liang, X.H. Liu, L.-Q. Chen, J.Y. Huang, J. Li, T. Zhu, S. Zhang, Nano Lett. 12 (2012) 1953–1958.
[27] K.Q. Peng, J.J. Hu, Y.J. Yan, Y. Wu, H. Fang, Y. Xu, S.T. Lee, J. Zhu, Adv. Funct. Mater. 16 (2006) 387–394.
[28] K.Q. Peng, Y. Wu, H. Fang, X.Y. Zhong, Y. Xu, J. Zhu, Angew. Chem. Int. Ed. 44 (2005) 2737–2742.
[29] G.L. Clark, Applied X-rays, third ed., McGraw-Hill, New York, 1940. pp. 122–125.
[30] Y. Sobajima, S. Nakano, T. Toyama, H. Okamoto, S. Omae, T. Minemoto, H. Takakura, Y. Hamakawa, J. Appl. Phys. 101 (2007) 103537.
[31] L.F. Cui, Y. Yang, C.M. Hsu, Y. Cui, Nano Lett. 9 (2009) 3370–3374.
[32] Y.S. Hu, P. Adelhelm, B.M. Smarsly, J. Maier, ChemSusChem 3 (2010) 231–235.
[33] Y.H. Xu, G.P. Yin, Y.L. Ma, P.J. Zuo, X.Q. Cheng, J. Mater. Chem. 20 (2010) 3216–3220.
[34] Q. Si, K. Hanai, T. Ichikawa, A. Hirano, N. Imanishi, Y. Takeda, O. Yamamoto, J. Power Sources 195 (2010) 1720–1725.
[35] W. Wang, P.N. Kumta, ACS Nano 4 (2010) 1443–1450.
[36] S. Murugesan, J.T. Harris, B.A. Korgel, K.J. Steveson, Chem. Mater. 24 (2012) 1306–1315.
[37] S.D. Beattie, D. Larcher, M. Morcrette, B. Simon, J.-M. Tarascon, J. Electrochem. Soc. 155 (2008) A158–A163.
[38] B. Koo, H. Kim, Y. Cho, K.T. Lee, N.-S. Choi, J. Cho, Angew. Chem. Int. Ed. 51 (2012) 8762–8767.